Received: 1 June 2022 | Revised: 5 July 2022 | Accepted: 31 July 2022

DOI: 10.1111/ijac.14186

International Journal of Applied Ceramic Technology

SPECIAL ISSUE ARTICLE

Impact of blending with polystyrene on the microstructural and electrochemical properties of SiOC ceramic

Monika Wilamowska-Zawlocka[1] | **Magdalena Graczyk-Zajac**[2,3]

[1]Department of Energy Conversion and Storage, Faculty of Chemistry, Gdańsk University of Technology, Gdańsk, Poland

[2]EnBW Energie Baden-Württemberg AG, Karlsruhe, Germany

[3]Institut für Materialwissenschaft, Technische Universität Darmstadt, Darmstadt, Germany

Correspondence
Magdalena Graczyk-Zajac, EnBW Energie Baden-Württemberg AG, Karlsruhe, Germany.
Email: m.graczyk-zajac@enbw.com

Funding information
BEETHOVEN CLASSIC 3 program of The National Science Centre, Grant/Award Number: UMO-2018/31/G/ST5/02056; Horizon 2020 project SIMBA, Grant/Award Number: 963542; DFG, Grant/Award Number: GR 4440/4-1

Abstract

In this work, we present the electrochemical behavior and microstructural analysis of silicon oxycarbide (SiOC) ceramics influenced by an addition of polystyrene (PS). Polymer-derived ceramics were obtained by pyrolysis (1000°C, Ar atmosphere) of different polysiloxanes prepared by sol–gel synthesis. This method is very effective to obtain desired composition of final ceramic. Two alkoxysilanes phenylthriethoxysilane and diphenyldimethoxysilane were used as precursors. Before pyrolysis polysiloxanes were mixed with PS using toluene as a solvent. Blending with PS affects the microstructure and free carbon content in the final ceramic material. Free carbon phase has been confirmed to be a major lithium storage host. Nevertheless, we demonstrate here that capacity does not increase linearly with increasing carbon content. We show that the amount of SiO_4 units in the SiOC microstructure increases the initial capacity but decreases the cycling stability and rate capability of the material. Furthermore, the microstructure of the free carbon influences the electrochemical performance of the ceramic: More ordered graphitic clusters favor better rate capability performance.

KEYWORDS
carbon organization, lithium-ion battery, polymer-derived ceramic, silicon oxycarbide

1 | INTRODUCTION

Lithium-ion batteries are widely used in all aspects of our modern life from portable electronic devices to electric vehicles and even to military and space applications due to its high energy density, high voltage, low self-discharge rate, and no memory effect. Currently graphite with a theoretical capacity of 372 mA h g^{-1} is used as anode in most commercial lithium-ion batteries. The capacity and the charge rate capability of graphite are nevertheless far from meeting the demand for high-performance lithium-ion batteries.[1–3] Silicon appears to be a promising candidate to replace graphite due to its super high theoretical capacity of ~3600 mA h g^{-1}, which is almost 10 times higher compared with graphite anode, low discharge potential (.5 V vs. Li/Li^+), and abundant reserves. Nevertheless, ~300% volume expansion of silicon during lithiation and accompanying phase transformation causes a pulverization of the material and delamination of the electrode, thus leading to a fast fading of capacity and low Coulombic efficiency. Although many solutions for enhancing electrochemical performance of Si-based anode such as nanosizing of Si and Si-conductive coating composites have been addressed, from a commercial and practical

point of view, only anodes with a fraction of elemental silicon (up to 10–15 wt.%) present a stable electrochemical behavior[4–6] (refer to Tesla announcement September 2020).

Si-based polymer-derived ceramics (PDCs) like silicon oxycarbide (SiOC) and silicon carbontride (SiCN) gained extensive attention as potential anode materials for LIB due to their unique temperature-dependent amorphous microstructure at relatively low pyrolysis temperatures (~up to 1100°C for SiOC and ~up to 1300°C for SiCN) under an inert or reactive atmosphere. Crystallization up to around 1300–1500°C can be resisted due to the graphene-like sp^2 bonded carbon network atoms located at the boundary of tetrahedral nanodomains of silicon. This character results in an excellent chemical and thermodynamic stability, elevated electrical conductivity (6×10^{-3} S cm^{-1}), as well as robust mechanical properties. Moreover, a remarkable number of works have demonstrated that PDCs materials can reversibly store Li with high electrochemical capacities up to 650 mA h g^{-1} and with Coulombic efficiencies over 99%. All these benefits make PDCs materials possible to be anodes for LIB. Besides, all previous properties, including porosity, can easily be adjusted by chemical modification and tunable parameters, which makes it easier to meet the requirement as people wish.[7–10]

In 1994, Wilson et al. reported for the first time on electrochemical properties of a polymer-derived SiOC pyrolyzed from siloxane in terms of a reversible lithium intercalation. This work revealed that SiOC ceramics accept lithium ions at potential lower than 1 V with a high specific capacity close to 600 mA h g^{-1}. The study of the effect of processing temperature on a cycle stability of SiOC anode demonstrates the lowest first cycle loss and highest reversible capacity for samples pyrolyzed at 1000°C.[11] The further works of Dahn's group focused on the effect of chemical concentrations on electrochemical performance by over 60 different SiOC materials, with the composition 14% Si and 80% C revealing the best electrochemical performance.[12] Although those works focused on the impact of the elemental composition on the electrochemical behavior, they did not address the mechanism of lithium storage and lithium transport.[13–17] The works of Saha et al. and Ahn et al. claimed that the major lithiation site is the mixed bond configuration (tetrahedrally coordinated silicon from SiC_4 via SiC_3O, SiC_2O_2, and $SiCO_3$ to SiO_4).[18–20] On contrary to these findings, Fukui et al.,[21,22] Graczyk-Zajac,[23] Dibandjo,[24] and Pradeep[25–32] demonstrated that the free carbon phase is the major Li-ion storage host site due to the interstitial and defect sites, edges of graphene sheets, porosity, and interfacial adsorption on the interface of graphite nanocrystallites, which result in effective storage of Li ions in SiOC ceramics. ^{7}Li MAS NMR spectra (nuclear magnetic resonance) measurements were applied to confirm that carbon phase is the host site for lithium storage by Fukui et al.[22] and Haaks et al.[33] The Riedel's group investigated polyorganosiloxane-derived SiOC anode pyrolyzed at temperatures from 900 to 2000°C by and demonstrated that the reversible capacity decreases with the rise of pyrolysis temperature and crystalline SiC is formed when the processed temperature over 1200°C (660 mA h g^{-1} for 900°C to 80 mA h g^{-1} for 2000°C).[34] The effect of electrical conductivity on capacity of SiOC was also addressed in the following work of the same group, revealing that low carbon content exhibits high initially capacities but fades rapidly in following cycling, and over 20-wt.% carbon content is beneficial for the conductivity and cycling stability.[35]

Porous SiOC materials have also been investigated as promising materials for Li-ion battery. Dibandjo et al. studied the difference between dense and porous SiOC anodes and found that the porous sample exhibits more stable electrochemical performance.[36] Pradeep et al. synthesized a linear polysiloxane cross-linked with divinylbenzene by hydrosilylation reaction catalyzed by Pt. After pyrolysis at 1000°C under argon, the obtained porous SiOC with 180 m^2 g^{-1} of specific surface area exhibits a high specific capacity over 600 mA h g^{-1} due to the porous structure providing enough fast ionic transport paths and accommodating the structural changes.[29] Fukui et al. developed a microporous SiOC composite material by pyrolyzing a blend of polysilane at 1000°C, which shows a remarkable capacity of 600 mA h g^{-1} and a good cycle stability.[37] Xia et al. studied the impact of etching SiOC by KOH and found an improved specific area of the material and enhanced the performance of the anode.[38]

In the present work, we investigate the impact of polymer blending with polystyrene (PS) on the microstructural and electrochemical properties of the final ceramic.

2 | EXPERIMENTAL SECTION

2.1 | Synthesis of the materials

SiOC samples were obtained by the pyrolysis of polysiloxanes synthesized by a sol–gel method. The synthesis procedure was as follows: High purity phenyltriethoxysilane (Sigma-Aldrich, Germany) (sample phenylthriethoxysilane [PhTEOS]) or diphenyldimethoxysilane (DPhDMOS) (Sigma-Aldrich, Germany) (sample DPhDMOS) was mixed with alcohol (Avantor Performance Materials Poland S.A.) (EtOH in the case of PhTEOS and MeOH in the case of DPhDMOS) (alcohol/Si = 2) and co-hydrolyzed with acidic water

(pH = 4.5, acidified with HCl [Avantor Performance Materials Poland S.A.]) using its stoichiometric amount (1 mol of H^+/H_2O per 1 alkoxy group, namely, 3 mol of H^+/H_2O per 1 mol of PhTEOS, and 2 mol of H^+/H_2O per 1 mol of DPhDMOS). The acidic water was added dropwise to the alkoxysilane/alcohol solution. Then, the mixture was heated to the boiling point and refluxed for 1 h. The resulting sols were cooled to the room temperature, transferred to the polypropylene test tubes, and left for gelation and drying processes (2 days at room temperature, 2 days at 40°C, 2 days at 60°C, 2 days at 80°C, 2 days at 100°C, and 2 days at 120°C). To obtain the final ceramics, the dried gels were pyrolyzed under argon atmosphere with the heating rate of 100°C h^{-1} from a room temperature to the final temperature (1000°C, dwell time 1 h), and cooling with the same rate to a room temperature. To obtain the samples with PS addition, the dried gels (PhTEOS, DPhDMOS) were dissolved in toluene (Avantor Performance Materials Poland S.A.) and mixed with PS (Sigma-Aldrich, Germany) in the 1:1 weight ratio (samples PhTEOS:PS, DPhDMOS:PS). Then, the toluene was evaporated, and the gels were dried (2 days at 100°C, 2 days at 120°C). The dried polysiloxane/PS blends were pyrolyzed with the same parameters as the pure polysiloxanes.

2.2 | Electrochemical cells preparation

The investigated SiOC samples were milled in the ball mill (MM200, Retsch, Germany) to obtain powder with median particle size of 10 μm and D90 below 40 μm. The composite electrodes were obtained from the slurry comprising 85 wt.% of active material (SiOC sample), 10 wt.% of binder polyvinylidene fluoride (Solef 6020, Solvay, Germany) dissolved in *N*-methyl 2-pyrrolidone (BASF, Germany) and 5 wt.% of conductive additive Carbon Black Super P (Imerys Graphite & Carbon, Switzerland), and ~1–1.2 g of NMP to adjust viscosity. The slurry was casted on a copper foil (10 μm, Copper SE-Cu58 Schlenk Metallfolien GmbH& Co. KG, Germany) using a doctor blade technique. The obtained electrode layers were then dried at 80°C for 24 h, cut into circles of 10 mm in diameter, weighted, dried under vacuum at 80°C for 24 h, and transferred into glove box (Mbraun Glove Box Systems, Ar atmosphere, below .5 ppm of H_2O, below .5 ppm of O_2) without contact with air.

For electrochemical tests, Swagelok type two-electrode cells were assembled with SiOC samples as working electrodes and lithium foil (Sigma-Aldrich, Germany) as counter/reference electrode. The electrolyte was 1-M $LiPF_6$ in ethylene carbonate:dimethyl carbonate (1:1 v/v, Sigma-Aldrich, Germany). A quartz filter paper (GF-2, 45-μm thick, Macherey-Nagel GmbH & Co. KG, Germany) was used as a separator.

2.3 | Electrochemical measurements

Galvanostatic cycling was performed using multichannel battery tester (Atlas 0961, Atlas-Sollich, Poland), and potentiostat–galvanostat (SP200, BioLogic Science Instruments, France). The potentials were set between 3.0 and .005 V at different current rates, charge currents were the same as discharge currents $C = D$ ($C/20 = 18.6$ mA g^{-1}, $C/10 = 37.2$ mA g^{-1}, $C/5 = 74.4$ mA g^{-1}, $C/2 = 186$ mA g^{-1}, $C = 372$ mA g^{-1}, and $2C = 744$ mA g^{-1}). The current rates and capacities were calculated per mass of active material.

3 | RESULTS AND DISCUSSION

Figure 1 shows a schematic of the preparation of ceramic material, pristine and blended with PS. Two alkoxysilanes each containing a different amount of phenyl group in the structure are used as ceramic precursors: PhTEOS and DPhDMOS. To increase the amount of free carbon and to modify the morphology of the final ceramic material, PS has been blended with the xerogel using toluene as a solvent. Four ceramic materials have been chosen for the further study: Pristine material derived from PhTEOS and its blend 1:1 in wt.% with PS, PhTEOS:PS; and pristine material derived from DPhDMOS, and its blend 1:1 with PS, DPhDMOS:PS.

Phenyltriethoxysilane was selected, based on our previous studies, because of high carbon content and good electrochemical performance of the PhTES-based SiOC ceramic.[31] The aim of our studies is to find correlation between organic functional groups attached to the preceramic polymer chains and the microstructure, chemical composition, and the resulting electrochemical performance of the ceramic samples. Polysiloxanes obtained from DPhDMOS have a low ceramic yield (see TGA in Figure S1). However, this precursor was investigated due to two carbon-rich organic groups attached to one silicon atom, and therefore, expected high share of mixed bonds silicon tetrahedra, and high carbon content in the final ceramic. The results of the elemental analysis are gathered in Table 1. As a result of the PS addition, the amount of free carbon increases in the final ceramic of about 2–3 wt.%. PS decomposes above 400°C; therefore, it does not contribute much to the carbon content. However, PS in the preceramic polymer blend may influence the structure and porosity of the final ceramic product.[39]

Microstructural evolution of the ceramic material in the presence of graphite has been evaluated using Raman

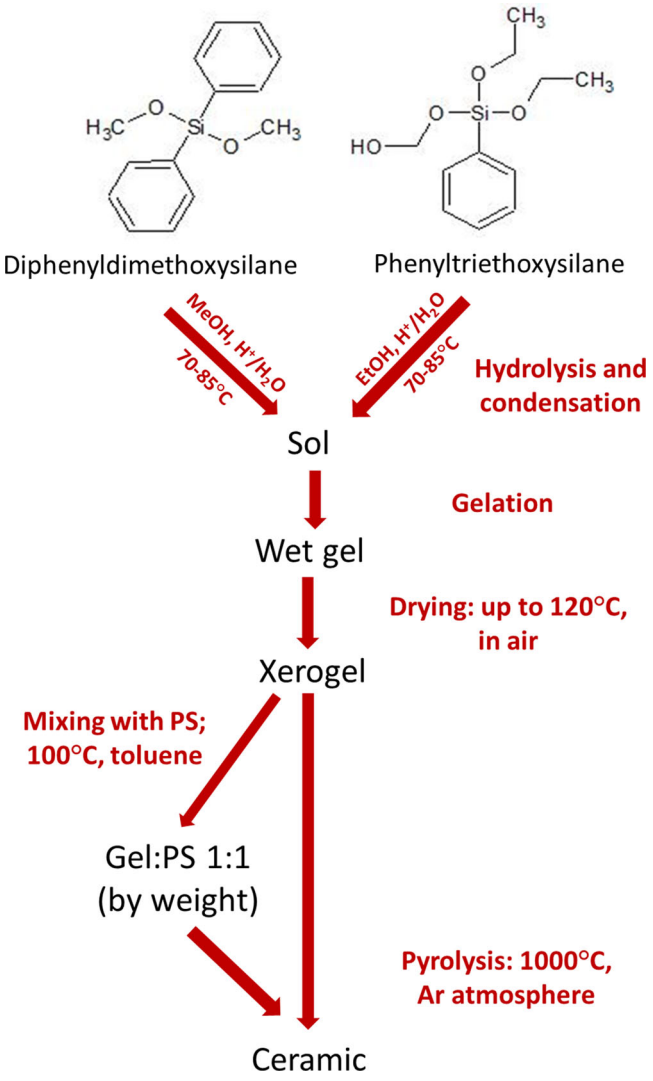

FIGURE 1 Schematic representation of the synthesis of pristine ceramics and ceramic—polystyrene (PS) composites

TABLE 1 Elemental composition of the investigated ceramic materials

Material	Si* wt.%	O	C	C_{free}	Empirical formula
PhTEOS	31.3	29.1	39.6	37.2	$SiO_{1.63}C_{2.96}$
PhTEOS:PS	29.7	27.0	43.3	40.6	$SiO_{1.59}C_{3.39}$
DPhDMOS	25.9	23.2	50.9	48.6	$SiO_{1.57}C_{4.60}$
DPhDMOS:PS	24.4	23.0	52.6	50.8	$SiO_{1.66}C_{5.04}$

Abbreviations: DPhDMOS, diphenyldimethoxysilane; PhTEOS, phenylthriethoxysilane; PS, polystyrene.

spectroscopy (Figure 2). The spectra of all investigated samples reveal two characteristic bands: The D band, at around 1329 ± 1 cm^{-1}, originating from disordered graphene layers and the G band at around 1590 ± 10 cm^{-1}, which corresponds to ideal graphitic lattice [ref]. Bands around 2685 ± 20 and 2900 ± 20 cm^{-1} represent overtones of D mode and combination of D + G bands, respectively.[33,34] In order to get more insights into the microstructural features of the investigated samples, the first-order spectra have been deconvoluted.[33–35] The deconvolution reveals one additional bands D3 related to amorphous carbon.[33] The example of a deconvoluted spectrum is shown in the inset in Figure 2. Moreover, the details such as bands positions, intensity, area, and intensity ratio I_{D1}/I_G obtained from the fitting of the Raman spectra of the investigated samples are gathered in Table 2. The analysis of the deconvoluted Raman spectra reveals a decrease of I_{D1}/I_G from 5.2 to 4.6 for PhTEOS and DPhDMOS and from 5.4 to 3.9 for PhTEOS:PS and DPhDMOS:PS, respectively. This is attributed to the increasing intensity of G band due to the increasing share of ordered graphitic clusters in the carbon phase, possibly originating from increased amount of the free carbon phase.

^{29}Si MAS NMR spectra of PhTEOS and DPhDMOS derived ceramic and their blend with PS are shown in Figure 3, whereas the results of the spectra deconvolution are summarized in Table 3. Surprisingly, blending with PS leads to a decrease of $\underline{Si}O_4$ units in the PhTEOS-derived material (from 76% to 70.4%), whereas in the case of DPhDMOS, initially containing much lower amount of $\underline{Si}O_4$ units, its percentage increases from 47.8% to 65.7%, whereas the amount of SiO_3C and SiO_2C_2 diminishes. Note that in both materials, PhTMOS and DPhDMOS, blending with PS leads to the increase of the amount of the free carbon phase of ca. 2%.

3.1 | Electrochemical performance

Figure 4A,B shows the first lithiation–delithiation curves and a discharge capacity versus cycle number of SiOC electrodes recorded at different current rates, respectively.

In the first cycle of PhTEOS, the longest plateau is found at .4 V, whereas for other samples the plateau is more "sloping." In parallel, PhTEOS-derived ceramic reveals the lowest reversible capacity of 652 mA h g^{-1}. This is rationalized by the highest percentage of SiO_4 units, as revealed by ^{29}Si ssNMR, compare Table 3. The more silica-rich the material is, the more pronounced the plateau, which we attribute to a hardly reversible storage of lithium ions in the proximity of oxygen in a silica-rich environment. As Li–O interaction is strong,[40] Li ions remain in the silica-rich environment and the capacity tends to fade. A similar plateau at ∼.25 V was observed, when inserting lithium ions into SiO*x*-based electrodes,[41] which confirms this hypothesis. The highest first cycle Coulombic efficiency is found for DPhDMOS material, namely, 61.6%; however, no significant difference is found in the

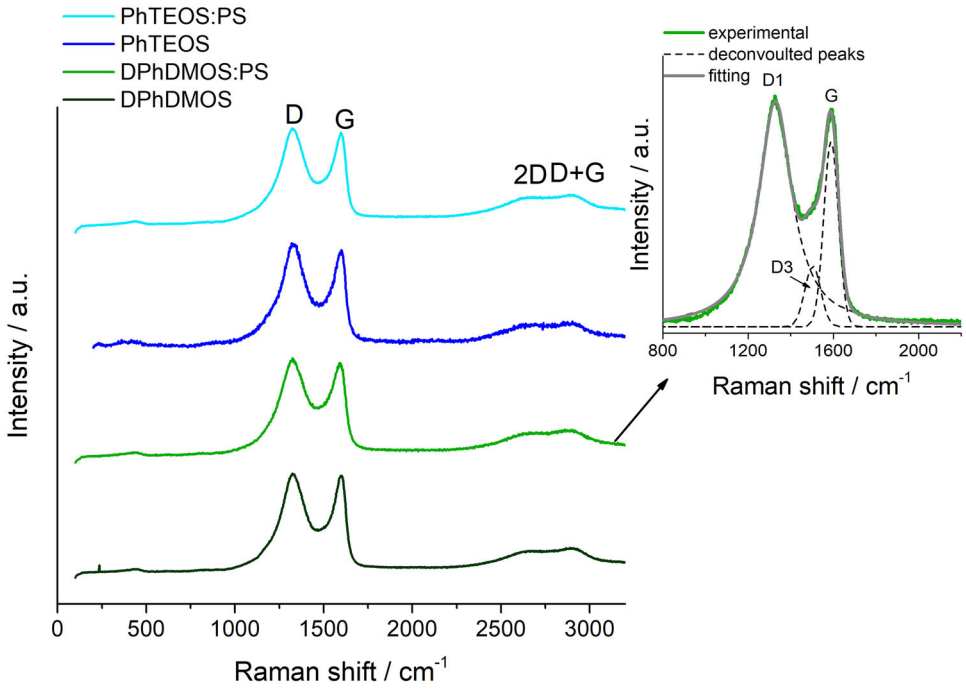

FIGURE 2 Raman spectra of the investigated ceramics, in the inset an example of the spectrum deconvolution

TABLE 2 Position of D1, D3, and G peaks in Raman spectra of analyzed samples and calculated relative areas of these peaks and the corresponding ratio of I_{D1}/I_G peak areas

Sample	D1 (cm^{-1})	D3 (cm^{-1})	G (cm^{-1})	Peak area (%)			I_{D1}/I_G
				D1	D3	G	
PhTEOS	1329	1536	1598	71.4	14.9	13.8	5.2
PhTEOS:PS	1328	1528	1598	74.7	9.5	15.8	5.4
DPhDMOS	1330	1531	1599	73.1	10.9	15.9	4.6
DPhDMOS:PS	1328	1503	1589	74.1	6.8	19.1	3.9

Abbreviations: DPhDMOS, diphenyldimethoxysilane; PhTEOS, phenylthriethoxysilane; PS, polystyrene.

TABLE 3 Results of a deconvolution of the 29Si MAS NMR spectra

Sample	Si site (%)					
	SiO_4	δ (ppm)	SiO_3C	δ (ppm)	SiO_2C_2	δ (ppm)
PhTEOS*	76	−104.6	16.4	−69.9	.6 7.1	−22.1 −38.2
PhTEOS:PS 1:1	70.4	−110	18.2	−76	11.4	−39
DPhDMOS	47.8	−111	33.1	−76	19.1	−37
DPhDMOS:PS 1:1	65.7	−106	25.8	−74	8.5	−43

Abbreviations: DPhDMOS, diphenyldimethoxysilane; PhTEOS, phenylthriethoxysilane; PS, polystyrene.

first insertion/extraction capacities among the investigated materials (compare Table 4).

The rate capability performance of the PhTEOS ceramic is also the lowest among the investigated materials with 165 mA h g^{-1} recovered with 2*C* rate. This test reveals significant differences in the performance of ceramics. Namely, the best results are registered for high carbon materials DPhDMOS and DPhDMOS:PS with the stable 241 and 219 mA h g^{-1} recovered at 2*C* rate and much lower capacities recovered by PhTEOS:PS with 193 mA h g^{-1} (40.6-wt.% C_{free}) and 165 mA h g^{-1} by PhTEOS sample containing 37.2 wt.% of free carbon.

Nevertheless, the enhanced electrochemical performance of DPhDMOS-derived materials cannot only be

TABLE 4 Irreversible capacities C_{irrev}, first cycle efficiencies, and average discharge capacities obtained at different current rates

Material	First cycle C_D (mA h g^{-1})			140th cycle	Average discharge capacity (mA h g^{-1})		
	C_{irrev}	$C/20$	Efficiency (%)	$C/20$	$C/2$	C	$2C$
PhTEOS	422	652	60.7	495	299	232	165
PhTEOS:PS	451	719	61.4	552	410	305	193
DPhDMOS	412	663	61.6	577	436	349	241
DPhDMOS:PS	472	680	59.0	533	400	320	219

Abbreviations: DPhDMOS, diphenyldimethoxysilane; PhTEOS, phenylthriethoxysilane; PS, polystyrene.

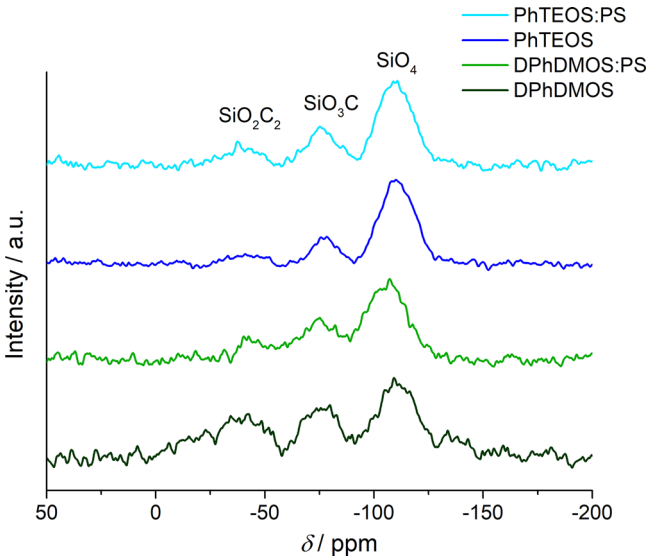

FIGURE 3 ^{29}Si MAS NMR spectra of all silicon oxycarbide (SiOC) samples

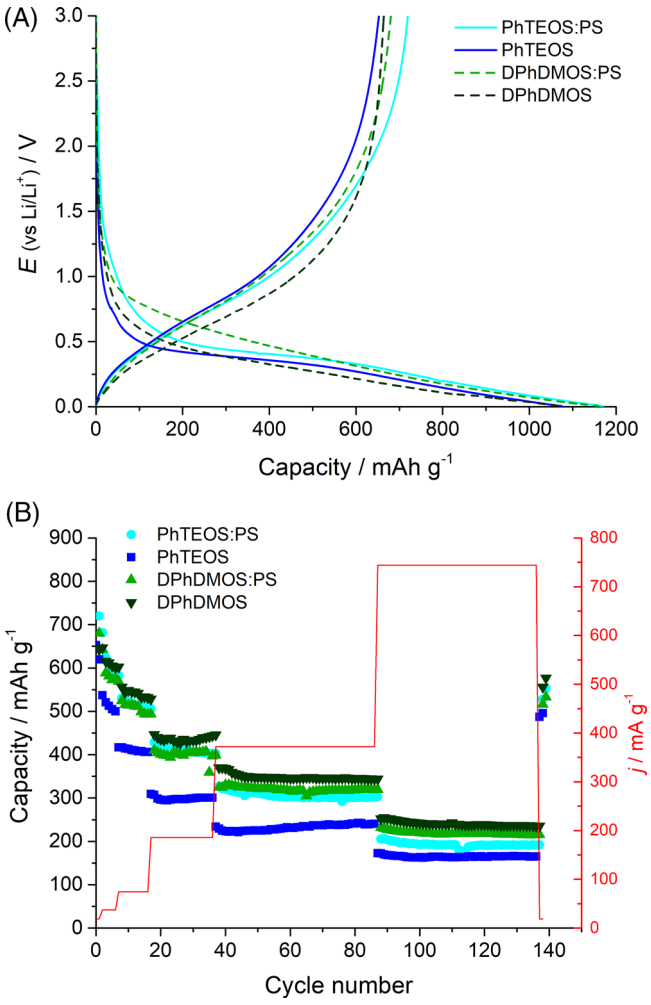

FIGURE 4 First lithiation/delithiation cycle of silicon oxycarbide (SiOC) electrodes (A) and discharge capacity versus (B) cycle number of SiOC electrodes recorded at different current rates

rationalized by the amount of the free carbon phase. Note that the I_{D1}/I_G ratio for the best performing materials is significantly lower than the one calculated for PhTEOS-derived materials. The lower I_{D1}/I_G signifies an increasing share of ordered graphitic clusters in the carbon phase, which possibly leads to a better electrochemical performance of the materials. Moreover, both the DPhDMOS-derived samples exhibit higher amount of mixed bonds silicon tetrahedra (SiO_3C and SiO_2C_2) compared to PhTES-based materials. These observations suggest a noticeable influence of microstructure on the reversible lithium insertion of the materials.

4 | CONCLUSIONS

Within this work, we evaluate sol–gel-derived PhTOES and DPhDMOS-derived ceramics and their composites with PS for potential application as anodes in lithium-ion batteries. The focus of the work is on identifying how the change of the ceramic microstructure induced by blending with PS affects the storage of lithium ions. The material with a lower carbon content and a high percentage of SiO_4 units shows initially fair capacities comparable to ceramics with a higher carbon content; however, it performs much worse during a rate capability tests. For a stable and reversible lithium storing performance, both at high and low currents, ceramics containing more than 40 wt.% of a free carbon phase show advantageous behavior. The

ordering of graphitic clusters and high share of mixed bonds silicon tetrahedra seem to enhance the performance of ceramics at higher currents.

ACKNOWLEDGMENTS

MWZ acknowledges financial support from BEETHOVEN CLASSIC 3 program of The National Science Centre (Project "Beyond Li-ion batteries: On novel and Efficient electrode materials for Sodium Storage," Grant no. UMO-2018/31/G/ST5/02056). MGZ acknowledges EU support within Horizon 2020 project SIMBA (sodium-ion and sodium metal batteries for efficient and sustainable next-generation energy storage) under Grant agreement number 963542 and DFG support in the frame of the project GR 4440/4-1.

Open access funding enabled and organized by Projekt DEAL.

ORCID

Monika Wilamowska-Zawlocka https://orcid.org/0000-0002-3618-1435
Magdalena Graczyk-Zajac https://orcid.org/0000-0002-4283-6549

REFERENCES

1. Wu F, Maier J, Yu Y. Guidelines and trends for next-generation rechargeable lithium and lithium-ion batteries. Chem Soc Rev. 2020;49(5):1569–614.
2. Kim T, Song W, Son D-Y, Ono LK, Qi Y. Lithium-ion batteries: outlook on present, future, and hybridized technologies. J Mater Chem A. 2019;7(7):2942–64.
3. Choi JW, Aurbach D. Promise and reality of post-lithium-ion batteries with high energy densities. Nat Rev Mater. 2016;1:16013.
4. Lu J, Chen Z, Pan F, Cui Y, Amine K. High-performance anode materials for rechargeable lithium-ion batteries. Electrochem Energy Rev. 2018;1(1):35–53.
5. Feng K, Li M, Liu W, Kashkooli AG, Xiao X, Cai M, et al. Silicon-based anodes for lithium-ion batteries: from fundamentals to practical applications. Small. 2018;14(8):1702737 (1–33).
6. Zuo X, Zhu J, Müller-Buschbaum P, Cheng Y-J. Silicon based lithium-ion battery anodes: a chronicle perspective review. Nano Energy. 2017;31:113–43.
7. Viard A, Fonblanc D, Lopez-Ferber D, Schmidt M, Lale A, Durif C, et al. Polymer derived Si-B-C-N ceramics: 30 years of research. Adv Eng Mater. 2018;20(10):1800360.
8. Mera G, Gallei M, Bernard S, Ionescu E. Ceramic nanocomposites from tailor-made preceramic polymers. Nanomaterials. 2015;5(2):468–540.
9. Graczyk-Zajac M, Reinold LM, Kaspar J, Sasikumar PVW, Soraru G-D, Riedel R. New insights into understanding irreversible and reversible lithium storage within SiOC and SiCN ceramics. Nanomaterials. 2015;5(1):233–45.
10. Knozowski D, Graczyk-Zajac M, Trykowski G, Wilamowska-Zawlocka M. Silicon oxycarbide-graphite electrodes for high-power energy storage devices. Materials. 2020;13(19):4302.
11. Wilson AM, Reimers JN, Fuller EW, Dahn JR. Lithium insertion in pyrolyzed siloxane polymers. Solid State Ionics. 1994;74(3–4):249–54.
12. Xing WB, Wilson AM, Eguchi K, Zank G, Dahn JR. Pyrolyzed polysiloxanes for use as anode materials in lithium-ion batteries. J Electrochem Soc. 1997;144(7):2410–6.
13. David L, Bhandavat R, Barrera U, Singh G. Polymer-derived ceramic functionalized MoS_2 composite paper as a stable lithium-ion battery electrode. Sci Rep. 2015;5:9792.
14. Xing WB, Wilson AM, Zank G, Dahn JR. Pyrolysed pitch-polysilane blends for use as anode materials in lithium ion batteries. Solid State Ionics. 1997;93(3–4):239–44.
15. Wilson AM, Zank G, Eguchi K, Xing W, Yates B, Dahn JR. Polysiloxane pyrolysis. Chem Mater. 1997;9(7):1601–6.
16. Wilson AM, Zank G, Eguchi K, Xing W, Dahn JR. Pyrolysed silicon-containing polymers as high capacity anodes for lithium-ion batteries. J Power Sources. 1997;68(2):195–200.
17. Wilson AM, Xing WB, Zank G, Yates B, Dahn JR. Pyrolysed pitch-polysilane blends for use as anode materials in lithium ion batteries .2. The effect of oxygen. Solid State Ionics. 1997;100(3–4):259–66.
18. Ahn D, Raj R. Cyclic stability and C-rate performance of amorphous silicon and carbon based anodes for electrochemical storage of lithium. J Power Sources. 2011;196(4):2179–86.
19. Sanchez-Jimenez PE, Raj R. Lithium insertion in polymer-derived silicon oxycarbide ceramics. J Am Ceram Soc. 2010;93(4):1127–35.
20. Saha A, Raj R, Williamson DL. A model for the nanodomains in polymer-derived SiCO. J Am Ceram Soc. 2006;89(7):2188–95.
21. Fukui H, Harimoto Y, Akasaka M, Eguchi K. Lithium species in electrochemically lithiated and delithiated silicon oxycarbides. ACS Appl Mater Interfaces. 2014;6(15):12827–36.
22. Fukui H, Ohsuka H, Hino T, Kanamura K. A Si-O-C composite anode: high capability and proposed mechanism of lithium storage associated with microstructural characteristics. ACS Appl Mater Interfaces. 2010;2(4):998–1008.
23. Graczyk-Zajac M, Toma L, Fasel C, Riedel R. Carbon-rich SiOC anodes for lithium-ion batteries: part I. Influence of material UV-pre-treatment on high power properties. Solid State Ionics. 2012;225:522–6.
24. Dibandjo P, Graczyk-Zajac M, Riedel R, Pradeep VS, Soraru GD. Lithium insertion into dense and porous carbon-rich polymer-derived SiOC ceramics. J Eur Ceram Soc. 2012;32(10):2495–503.
25. Pradeep VS, Graczyk-Zajac M, Riedel R, Soraru GD. New insights in to the lithium storage mechanism in polymer derived SiOC anode materials. Electrochim Acta. 2014;119:78–85.
26. Graczyk-Zajac M, Vrankovic D, Waleska P, Hess C, Sasikumar PV, Lauterbach S, et al. The Li-storage capacity of SiOC glasses with and without mixed silicon oxycarbide bonds. J Mater Chem A. 2018;6(1):93–103.
27. Knozowski D, Graczyk-Zajac M, Trykowski G, Wilamowska-Zawłocka M. Silicon oxycarbide-graphite electrodes for high-power energy storage devices. Materials. 2020;13(19):4302.
28. Kaspar J, Graczyk-Zajac M, Lauterbach S, Kleebe H-J, Riedel R. Silicon oxycarbide/nano-silicon composite anodes for Li-ion batteries: considerable influence of nano-crystalline vs. nano-amorphous silicon embedment on the electrochemical properties. J Power Sources. 2014;269:164–72.

29. Pradeep VS, Ayana DG, Graczyk-Zajac M, Soraru GD, Riedel R. High rate capability of SiOC ceramic aerogels with tailored porosity as anode materials for li-ion batteries. Electrochim Acta. 2015;157:41–5.
30. Pradeep VS, Graczyk-Zajac M, Riedel R, Soraru GD. New insights in to the lithium storage mechanism in polymer derived SiOC anode materials. Electrochim Acta. 2014;119:78–85.
31. Wilamowska M, Pradeep VS, Graczyk-Zajac M, Riedel R, Soraru GD. Tailoring of SiOC composition as a way to better performing anodes for Li-ion batteries. Solid State Ionics. 2014;260:94–100.
32. Knozowski D, Graczyk-Zając M, Vrankovic D, Trykowski G, Sawczak M, Carolis DMd, et al. New insights on lithium storage in silicon oxycarbide/carbon composites: impact of microstructure on electrochemical properties. Composites Part B: Eng. 2021;225:109302.
33. Haaks M, Kaspar J, Franz A, Graczyk-Zajac M, Riedel R, Vogel M. ^{7}Li NMR studies of lithium ion dynamics in polymer-derived silicon oxycarbide ceramics. Solid State Ionics. 2016;287:28–35.
34. Kaspar J, Graczyk-Zajac M, Riedel R. Lithium insertion into carbon-rich SiOC ceramics: influence of pyrolysis temperature on electrochemical properties. J Power Sources. 2013;244:450–5.
35. Kaspar J, Graczyk-Zajac M, Choudhury S, Riedel R. Impact of the electrical conductivity on the lithium capacity of polymer-derived silicon oxycarbide (SiOC) ceramics. Electrochim Acta. 2016;216:196–202.
36. Dibandjo P, Graczyk-Zajac M, Riedel R, Pradeep VS, Soraru GD. Lithium insertion into dense and porous carbon-rich polymer-derived SiOC ceramics. J Eur Ceram Soc. 2012;32(10):2495–503.
37. Fukui H, Ohsuka H, Hino T, Kanamura K. Preparation of microporous Si-O-C composite material and its lithium storage capability. Chem Lett. 2009;38(1):86–7.
38. Xia K, Wu Z, Xuan C, Xiao W, Wang J, Wang D. Effect of KOH etching on the structure and electrochemical performance of SiOC anodes for lithium-ion batteries. Electrochim Acta. 2017;245:287–95.
39. Fukui H, Ohsuka H, Hino T, Kanamura K. Influence of polystyrene/phenyl substituents in precursors on microstructures of Si-O-C composite anodes for lithium-ion batteries. J Power Sources. 2011;196(1):371–8.
40. Kroll P. Tracing reversible and irreversible Li insertion in SiCO ceramics with modeling and ab-initio simulations. MRS Online Proc Lib. 2011;1313:1–6.
41. Yamamura H, Nobuhara K, Nakanishi S, Iba H, Okada S . Investigation of the irreversible reaction mechanism and the reactive trigger on SiO anode material for lithium-ion battery. J Ceram Soc Jpn. 2011;119(1395):855–60.

SUPPORTING INFORMATION

Additional supporting information can be found online in the Supporting Information section at the end of this article.

How to cite this article: Wilamowska-Zawlocka M, Graczyk-Zajac M. Impact of blending with polystyrene on the microstructural and electrochemical properties of SiOC ceramic. Int J Appl Ceram Technol. 2022;1–8. https://doi.org/10.1111/ijac.14186